Potential of MEO SAR for Global Deformation Mapping

Jalal Matar[a], Marc Rodriguez-Cassola[a], Gerhard Krieger[a], Mariantonietta Zonno[a], and Alberto Moreira[a]
[a]Microwaves and Radar Institute, German Aerospace Center (DLR), 82334 Weßling, Germany

Abstract

Medium Earth Orbit (MEO) satellites have the ability to provide global coverage with 1- to 2-day revisit, at altitudes below 10000 km, and continental/oceanic coverage with multidaily observations at higher altitudes, e.g., at 20000 km. Increased altitudes provide more flexibility in the design of the observation geometry, e.g., going to highly inclined orbits while maintaining a global access, a favorable property for true 3-D deformation measurements with a monostatic system. Synthetic aperture radar (SAR) acquisitions from MEO altitudes require a certain compensation for the increased losses in the free space propagation of the radar signals and (typically) the coverage of wider swaths. These losses can be compensated by the usage of large antennas, high transmit powers, and a reduction in the spatial resolution. This paper discusses the potential of MEO-SAR systems to map ground deformation with high sensitivity to the North-South displacements at moderate resolutions (some tens of meters).

1 Introduction

Medium Earth Orbit (MEO) synthetic aperture radar (SAR) systems make use of the increased altitudes in order to cover wider swaths, 4-5 times larger than wide-swath Low Earth Orbit (LEO)-SAR systems. Going to higher altitudes limits the choice of orbits to non-sun-synchronous conditions. Unlike LEO systems which make use of sun-synchronous orbits in order to ensure a semi-continuous illumination from the Sun, MEO systems spend less time in the shadow of the Earth. Operating in a non-sun-synchronous orbit provides flexibility in the choice of orbital inclinations, allowing for an orbital design which provides an observation geometry sensitive to North-South displacements.

MEO-SAR systems require a certain compensation for the increased losses in the free space propagation of the radar signals and the coverage of wider swaths. The losses are partially compensated by the lower satellite velocities at higher altitudes, and the usage of longer antennas which are able to achieve higher resolution from higher orbital altitudes. This property is provided by the longer integration times linked to the reduction of the ratio between ground and spacecraft velocities, which reaches values close to 0.5 at around 6000 km [1]. The remaining losses can be further compensated by an increase in the transmit power, the usage of higher antennas for illuminating portions in the swath on transmission or reception. The former includes the use of burst operation modes (e.g., ScanSAR, TOPS) or multiple beam technologies, e.g., [2], [3], while the latter includes systems with scan-on-receive (SCORE) capabilities, e.g., [4]. The remaining losses are compensated by a reduction in the resolution, which makes a MEO-SAR system optimal for applications demanding high revisits and global coverage at moderate spatial resolutions (around 50 m) or alternatively multi-looked imagery with around 500-m resolutions. If desired MEO SAR can also deliver high-resolution imaging over narrow swaths with a reasonable system configuration, while maintaining the global access capability.

Land monitoring applications appear to be the perfect candidates for a MEO-SAR mission capable of performing true 3-D deformation measurements. From these we recall applications related to natural hazards and meteorology such as soil moisture and deformation estimation, e.g., volcanoes, active tectonics and landslides. Table 1 shows these applications and their corresponding system requirements.

Product	Spatial sampling	Temporal sampling	Traceability
Surface displacement (active tectonics & volcanoes)	50 m	3 d	[5], [6]
Land slides	50 m	3 d	[5], [6]
Soil moisture	1km	3 d	[6], [7], [8]

Table 1 Key land monitoring products and their corresponding requirements.

The structure of this paper is as follows. Section 2 shows the potential for performing differential SAR Interferometry (DInSAR) measurements from MEO. Section 3 presents a MEO-SAR mission suitable for hazard monitoring with sensitivity to North-South displacements. The paper is closed with a conclusion.

2 DInSAR measurements from MEO

The analysis is focused on repeat ground-track (RGT) orbits [9] which allow for repeat-pass interferometry by using different acquisitions over the same area at different times (repeat passes). Sun-synchronous repeat orbits are a special case of RGT orbits and are used by LEO-SAR systems to perform interferometric measurements. These orbits allow a semi-continuous illumination of the solar panels and are hence energy efficient, however, their existence is limited to polar inclinations at LEO altitudes. Moving to higher inclinations provide the observation geometry with sensitivity to North-South displacements, but can cause the loss of sun-synchronicity and a reduced coverage of the polar regions. These aspects become less problematic for higher altitude systems, e.g., MEO, as the spacecraft spends less time in the shadow of the Earth and can maintain a certain view of the polar regions. Figure 1 shows the coverage of a SAR instrument with [20° - 47°] incidence operating in an inclined 3/19 RGT MEO (repeating every 3 days after performing 19 revolutions). Non-sun-synchronous RGT orbits are subject to periods of orbital days (close to the sidereal day) with a difference in the order of few minutes compared to a civil day, causing systematic shifts in the acquisition times. These shifts provide samples at different times during the day, which can be exploited to capture not only seasonal, but also intradaily phenomena.

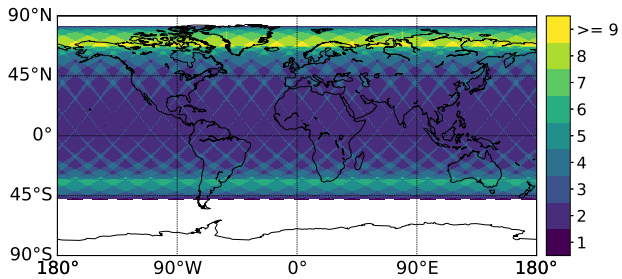

(a) Right looking geometry

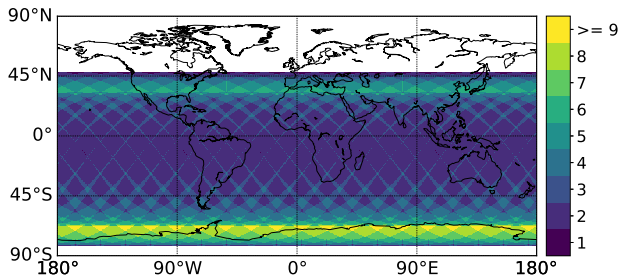

(b) Left looking geometry

Figure 1 Combined coverage (ascending and descending tracks) from a 3/19 RGT orbit with an inclination of 122° at 5952 km in (a) right-looking and (b) left-looking geometries. The swath corresponds to an incident angle range of [20° - 47°] and can cover 99% of the Earth's surface for combined left- and right-looking acquisitions.

The black arrows in Figure 2 show the projections of the line-of-sight (LOS) vectors on the ground for each of the ascending and descending passes of two right-looking SAR satellites, one near-polar LEO at 693 km (top-left) and another inclined MEO, here 122° at 5952 km (top right). The MEO clearly provides a better conditioned observation geometry since the projected LOS vectors have similar magnitudes in both the North and East directions. This is further demonstrated in the bottom plot of Figure 2, where the 1-D deformation accuracy is plotted against inclination. The convergence region in the plot, where all three displacement components are in the same order of magnitude, is of high interest for monitoring land deformation and hazards, since it allows for true 3-D deformation measurements using one satellite only, a feature which typically requires at least two spacecraft in LEO systems [10]. This allows for a better definition of the geometry and source of motion, which is required in order to correctly model and forecast future deformations and improve the assessment of the hazards arising from these phenomena.

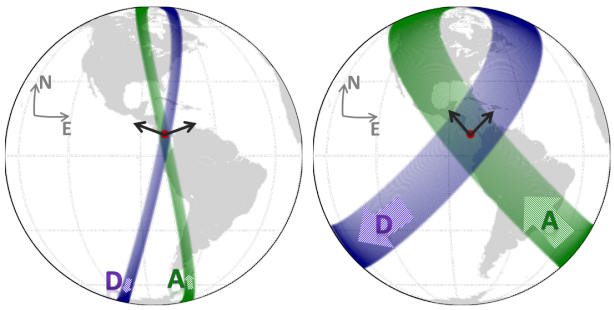

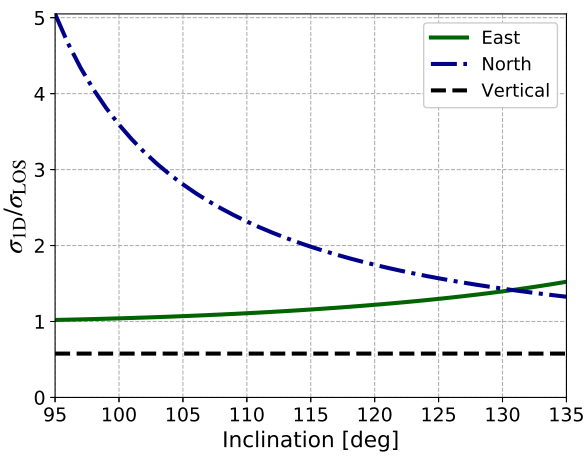

Figure 2 Projection of the LOS on the ground, represented by the black arrows, for a sun-synchronous LEO at 693 km (top-left) and a repeat MEO with 122° inclination at 5952 km (top-right). The green (labeled with an A) and blue (labeled with a D) swaths correspond to the right-looking ascending and descending satellite passes, respectively. The plot at the bottom represents the impact of changing the inclination on the achievable 3-D accuracy for an incident angle of 30° near the equator. σ_{1D} represents the deformation accuracy along a certain direction, e.g., Easting, Northing or Vertical, whereas σ_{LOS} represents the deformation accuracy along the line of sight [1].

3 Mission example DInSAR performance

In this section we provide a candidate orbit for a MEO-SAR mission targeting land monitoring applications on a global coverage scale and we assess its large scale deformation monitoring capability by means of DInSAR. The selected orbit at 5952 km altitude, with the orbital parameters listed in Table 2, is able to provide near global coverage (around 86% of the Earth's surface) for a [20° - 47°] incident angle range within 3 days only (ascending or descending track with a left- or right-looking geometry), and ensures an operation outside the peak radiation zones, mainly caused by the Van Allen belts. The poles are also accessible for an incident angle of 58°. A 122° inclination is suitable for achieving similar accuracies in the 3 directions of deformation as discussed in Section 2, and at the same time plays a role in the reduction to the 3 days revisit for global coverage with the given geometry. This is evident in Figure 3, where the variation of the northing angles along the swath is plotted for the ascending and descending passes in left- and right-looking geometries. The overlapped acquisitions from the different geometries, together with the near-orthogonal angles between the ascending and descending passes, allow for measuring 3-D deformations with uncertainties in the same order of magnitude. A detailed orbit selection strategy based on coverage scenarios, sensitivity, radiation environment and launch cost can be found in [1].

Orbit parameters	Value
Orbit type	repeat-ground-track
Repeat duration	3 days
Revolutions per repeat	19
Orbital altitude	5952 km
Inclination	122°
Eccentricity	0
Argument of perigee	90°
Right ascension of ascending node	359°
Orbital period	13624.7 sec

Table 2 Orbit parameters for a candidate MEO-SAR mission targeting global coverage.

Table 3 lists the main mission, atmosphere and instrument parameters used to carry out the performance analysis. The choice of L-band is justified by the ability of long wavelengths to provide long-term coherence in the estimation of slow surface deformations. The performance analysis was preceded by a mission timeline simulation, where every point on ground was assigned a time series of acquisitions with the corresponding geometries, for the entire mission duration. The DinSAR performance was then calculated using the hybrid Cramér-Rao bound (HCRB), described in [11]. An exponential model is assumed for the temporal decorrelation, with τ as the decorrelation time constant, γ_0 as the initial coherence term and γ_∞ as the persistent coherence term. The decorrelation due to the signal-to-noise ratio was calculated using the system's noise equivalent sigma zero (NESZ) and the backscattering values retrieved from the Global ALOS PALSAR backscattering map at L-band. The derivation of the DInSAR performance estimation for different systems is described in more detail in [10], [12].

Parameters	Value
Mission duration	4 years
Frequency	1.2575 GHz
Look directions	left & right
Incident angle range	[20° - 47°]
γ_0	0.9
γ_∞	0.1
Time constant τ	60 days
σ_{atm}	2 cm
σ_{iono}	1 cm
Product resolution	500 m x 500 m
Number of looks	< 100
NESZ	-26 dB
Backscattering map	Global ALOS PALSAR at L-band

Table 3 Parameters used in the DInSAR performance assessment.

Figure 4 shows the 2-D deformation accuracy maps in [mm/year] for regions labeled as high seismic hazard zones. The deformation uncertainty is estimated in all 3 directions, East-West, North-South and Up-Down, resulting in average values of 1.85 mm/year, 2.4 mm/year and 2.3 mm/year, respectively, over the previously mentioned hazard zones. The overlap between left- and right-looking acquisitions, for latitudes between $\pm 47°$, provide more distinct LOS geometries which reduces the maximum uncertainty to values below 3 mm/year in all directions. This accuracy is worsened when moving to higher latitudes, where only overlapped acquisitions from a single look are possible.

The results presented correspond to a 500 m $\times$ 500 m product resolution, and are obtained assuming 2 cm and 1 cm standard deviations for the atmospheric (σ_{atm}) and ionospheric (σ_{iono}) signal delays, respectively. The acquisitions used in the 4 years mission duration are divided into a 1 year of left-looking, 2 years of right looking and ended again with a 1 year of left-looking. The sensitivity to all directions of displacements combined with short revisit makes this example MEO-SAR mission a perfect candidate for hazard monitoring.

4 Conclusions

This paper discusses the potential of MEO-SAR systems to perform true 3-D motion and deformation measurements by operating at high inclinations without losing the global coverage capability with 1- to 2-day revisit. It also provides a candidate mission for hazard monitoring, which demonstrates the ability of a monostatic MEO-SAR system to perform DInSAR measurement with 3-D sensitivity, a feature hardly available to monostatic LEO systems.

5 Literature

[1] J. Matar, M. Rodriguez-Cassola, G. Krieger, P. López-Dekker, and A. Moreira. Meo sar: System concepts and analysis. *IEEE Transactions on Geoscience and Remote Sensing*, pages 1–12, 2019. doi: 10.1109/TGRS.2019.2945875.

[2] N. Gebert, G. Krieger, and A. Moreira. Multichannel Azimuth Processing in ScanSAR and TOPS Mode Operation. *IEEE Transactions on Geoscience and Remote Sensing*, 48 (7):2994–3008, 2010.

[3] F. De Zan and AM Guarnieri. TOPSAR: Terrain Observation by Progressive Scans. *IEEE Transactions on Geoscience and Remote Sensing*, 44(9):2352–2360, 2006.

[4] A. Freeman, G. Krieger, P. Rosen, M. Younis, W. Johnson, S. Huber, R. Jordan, and A. Moreira. SweepSAR: Beamforming on Receive using a Reflector-Phased Array Feed Combination for Spaceborne SAR. In *Radar Conference, 2009 IEEE*, pages 1–9. IEEE, 2009.

[5] M. Davidson et. al. Copernicus L-band SAR Mission Requirements Document. European Space Agency, 2018.

[6] W. Dorigo, W. Wagner, C. Albergel, F. Albrecht, G. Balsamo, D. Brocca, L. Chung, M. Ertl, M. Forkel, A. Gruber, et al. Esa cci soil moisture for improved earth system understanding: State-of-the art and future directions. *Remote Sensing of Environment*, 203:185–215, 2017.

[7] P. Bally. *Satellite Earth Observation for Geohazard Risk Management: The Santorini Conference, Santorini, Greece, 21-23 May 2012*. European Space Agency, 2014.

[8] World Meteorological Organization (WMO). Observing Systems Capability Analysis and Review Tool (OSCAR), 2020. URL `https://www.wmo-sat.info/oscar`.

[9] S. Vtipil and B. Newman. Determining an Earth Observation Repeat-Ground-Track Orbit for an Optimization Methodology. *Journal of Spacecraft and Rockets*, 49(1): 157–164, 2012.

[10] P. Prats-Iraola, P. Lopez-Dekker, F. De Zan, N. Yagüe-Martínez, M. Zonno, and M. Rodriguez-Cassola. Performance of 3-d surface deformation estimation for simultaneous squinted sar acquisitions. *IEEE Transactions on Geoscience and Remote Sensing*, 56(4):2147–2158, 2018. doi: 10.1109/TGRS.2017.2776140.

[11] A. M. Guarnieri and S. Tebaldini. Hybrid cramÉr–rao bounds for crustal displacement field estimators in sar interferometry. *IEEE Signal Processing Letters*, 14(12):1012–1015, 2007. doi: 10.1109/LSP.2007.904705.

[12] F. De Zan, P. Prats, and G. Krieger. Mission design and performance for systematic deformation measurements with a spaceborne sar system. In *2009 IEEE International Geoscience and Remote Sensing Symposium*, volume 2, pages II–793–II–796, 2009. doi: 10.1109/IGARSS.2009.5418212.

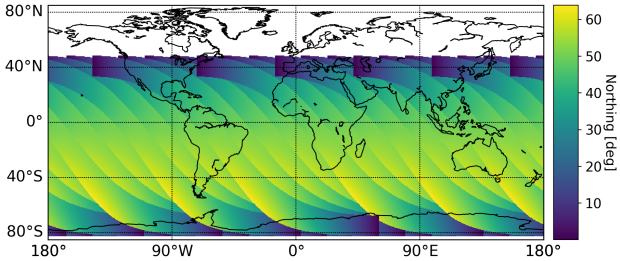

(a) Left looking - ascending

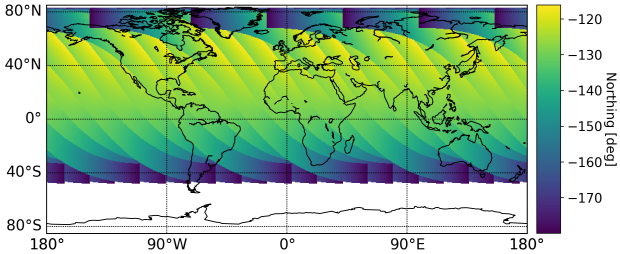

(b) Right looking - ascending

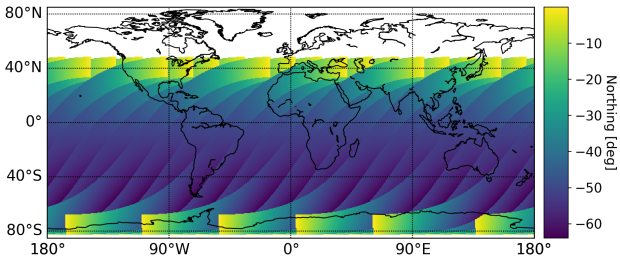

(c) Left looking - descending

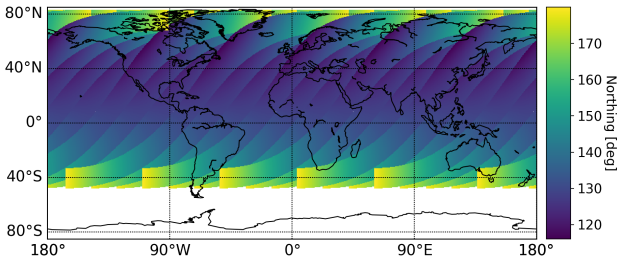

(d) Right looking - descending

Figure 3 Variation of the northing angles along the swath for the ascending pass in (a) left-looking geometry and (b) right-looking geometry, and for the descending pass in (c) left-looking geometry and (d) right-looking geometry.

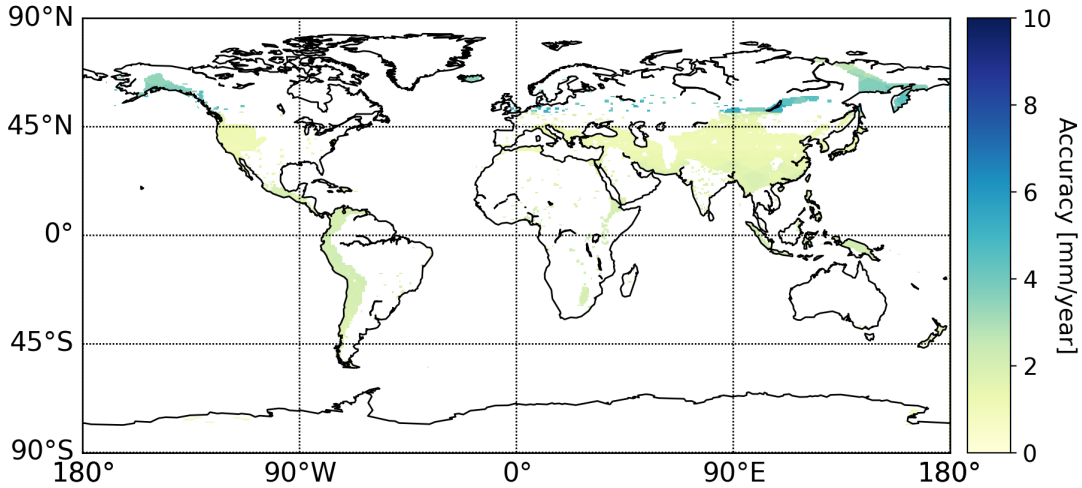

(a) East-West

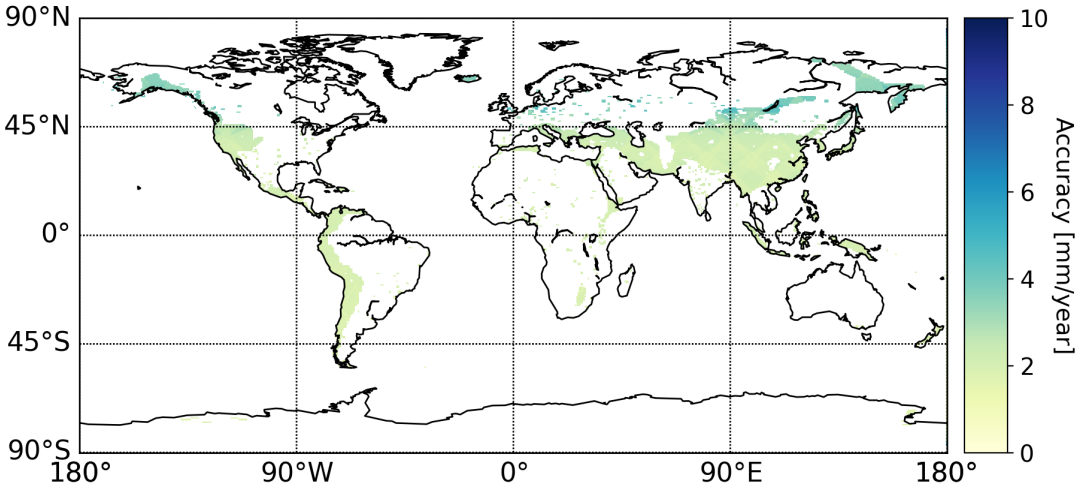

(b) North-South

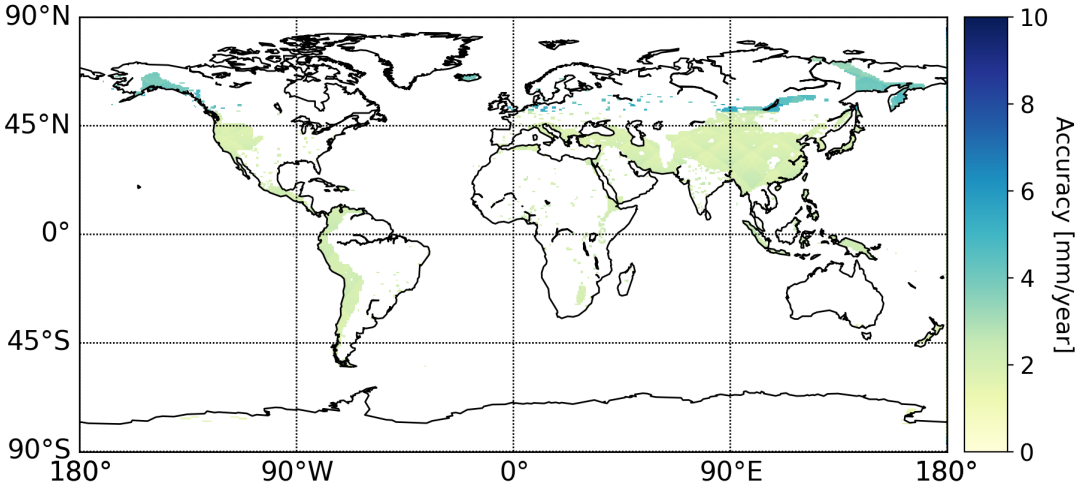

(c) Up-Down

Figure 4 Deformation accuracy maps in [mm/year], for regions labeled as high seismic hazard zones, in (a) East-West, (b) North-South and (c) Up-Down directions.